

Fluorine-18 Labeled Carboplatin Derivative for PET Imaging of Platinum Drug Distribution

Narottam Lamichhane^{1*}, Gajanan K. Dewkar^{1*}, Gobalakrishnan Sundaresan¹, Li Wang¹,
Purnima Jose¹, Muhammad Otabashi², Jean-Luc Morelle², Nicholas Farrell³, Jamal Zweit^{1,3}

¹Center for Molecular Imaging, Department of Radiology, Virginia Commonwealth University, 1101 E. Marshall Street, Richmond, Virginia 23298

²Trasis SA, Rue Gilles Magnee 90, 4430 Ans-Belgium

³Department of Chemistry, Virginia Commonwealth University, 1001 W. Main Street, Richmond, Virginia 23284

* Equal Contribution.

Correspondence Author:

Jamal Zweit, PhD, DSc

Center for Molecular Imaging, Department of Radiology

Virginia Commonwealth University

1101 E. Marshall Street, Sanger Hall, Room 8-022

Richmond, VA 23298-0031

Ph. No. (804) 628 2791

Fax. No. (804)-628-0223

E-mail: jamal.zweit@vcuhealth.org

First Authors

Narottam Lamichhane, PhD

Center for Molecular Imaging, Department of Radiology

Virginia Commonwealth University

1101 E. Marshall Street, Sanger Hall, Room 8-022

Richmond, VA 23298-0031

Ph. No. (484) 904 3099

Fax. No. (804)-628-0223

lamichhanen@vcu.edu

Gajanan K. Dewkar, PhD

Center for Molecular Imaging, Department of Radiology

Virginia Commonwealth University

1101 E. Marshall Street, Sanger Hall, Room 8-022

Richmond, VA 23298-0031

Ph. No. (732) 421 8046

Fax. No. (804)-628-0223

gdewkar@zevacor.com

Running Title: Fluorine-18 labeled Carboplatin PET

Word count: 4995

ABSTRACT

Increasing evidence indicates that reduced intracellular drug accumulation is the parameter most consistently associated with platinum drug resistance, and emphasizes the need to directly measure intra-tumor drug concentration. In the era of precision medicine and with the advent of powerful imaging and proteomics technologies, there is an opportunity to better understand drug resistance, by exploiting these techniques to provide new knowledge on drug-target interactions. Here, we are contributing to this endeavor by reporting on the development of a fluorine-18 labeled carboplatin derivative (^{18}F -FCP) that can be used to potentially image drug uptake and retention, including intra-tumoral distribution, by positron emission tomography (PET).

Methods: Fluorinated carboplatin (^{19}F -FCP) was synthesized using 2-(5-fluoro-pentyl)-2-methyl malonic acid (FPMA) as the labeling agent to coordinate with the cisplatin aqua complex. It was then used to treat cell lines and compared with cisplatin and carboplatin at different concentrations. Manual radio synthesis and characterization of ^{18}F -FCP was performed using ^{18}F -FPMA with coordination with cisplatin aqua complex. Automated radiosynthesis of ^{18}F -FCP was optimized based on the manual synthetic procedures. Stability of ^{18}F -FCP was verified using high performance liquid chromatography. ^{18}F -FCP was evaluated using *ex vivo* biodistribution and *in vivo* PET imaging in non-tumor animals as well as in KB 3-1 and COLO205 tumor xenograft bearing nude mice. **Results:** *In vitro* cytotoxicity studies demonstrated that ^{19}F -FCP has similar anti-tumor activity profile as the parent drug carboplatin. *In vivo* plasma and urine stability analysis showed intact ^{18}F -FCP at 24-hour post injection. PET imaging and biodistribution studies showed fast clearance

from blood and major accumulation in kidneys, indicating substantial renal clearance of ^{18}F -FCP. Using ^{18}F -FCP PET, we could image and identify intra-tumor drug profile.

Conclusion: Our results demonstrate that ^{19}F -FCP derivative, like carboplatin, retains anti-tumor activity in various cell lines. ^{18}F -FCP could be a useful imaging tool to measure intra-tumor drug distribution. This strategy of using new therapeutic carboplatin derivative to quantify and track platinum drugs in tumor using PET could potentially translate into a clinically useful imaging tool for individual patients.

Keywords: platinum, fluorinated carboplatin, PET, theranostics.

INTRODUCTION

Since the discovery of cisplatin by Rosenberg et al (1), platinum drugs have been a major chemotherapy treatment of cancer (2-5). In fact, platinum-based drugs are administered to nearly half of all cancer patients receiving chemotherapy (6). Despite some treatment efficacy of cisplatin and carboplatin chemotherapy, drug resistance, toxic side effects and tumor recurrence are still critical barriers that need to be addressed. Over the last several years, resurgence of platinum-based cancer chemotherapy has been driven by the development of new derivatives and by circumventing mechanisms of resistance, and thereby broadening the clinical use of these agents. Overcoming limitations of platinum drugs has stimulated further research towards understanding and improving platinum-based chemotherapy (6). Recent developments have also addressed novel strategies of targeting and better drug delivery approaches (7). Several mechanisms are implicated in tumor resistance to platinum drugs (8,9), and studies have revealed that reduced drug accumulation is most consistently associated with resistance, and emphasized the need to directly measure intra-tumor drug concentration (10). Contributing to this endeavor, we are reporting on the development of ^{18}F -FCP to image its distribution in tumors by PET. Such a noninvasive method may allow optimization of an individual's drug exposure at the tumor site, as well as provide a screening measure to determine efficacy in individual patients.

Previous strategies to synthesize radiolabeled platinum drugs, such as cis- and carboplatin, relied on the incorporation of a platinum isotope (e.g. ^{191}Pt , $^{195\text{m}}\text{Pt}$) as its chloride salt early in the drug synthesis (11-14). These studies provided valuable *in vivo*

data, but this approach could not be clinically translatable because of limited platinum radioisotope availability, long radio-synthesis and logistical cost. Another strategy used ^{13}N -cisplatin to assess pharmacokinetics in brain tumors (15,16). This method, however is limited by the ultra-short half-life (10 min) of ^{13}N . In this work, we sought to develop an alternative strategy by synthesizing ^{18}F -FCP. The rationale for the radiolabeling strategy is based on the coordination of platinum by malonic acid derivatives (17). We have previously developed a malonic acid precursor to produce ^{18}F -malonic acid derivative (18), which has been proposed as a potential PET apoptosis imaging agent (19). In this coordination-based labeling strategy, the fluorine isotope, ^{19}F or ^{18}F is introduced as a malonic acid derivative attached to the carboxylate group, which is subsequently replaced with water to form the active positively charged species. The widely-accepted mechanism of action of platinum agents considers the $\{\text{Pt}(\text{NH}_3)_2\}$ moiety in cisplatin or carboplatin to be the carrier group which binds to DNA upon eventual substitution of the chloride (cisplatin) or carboxylate (carboplatin) moiety. However, because of much slower aquation rate of carboplatin ($7 \times 10^{-7} \text{ s}^{-1}$) compared to cis-platin ($8 \times 10^{-5} \text{ s}^{-1}$), the rate of binding to DNA is also much slower for carboplatin (20), and therefore binding to DNA is expected to be slow, but compatible with the short half-life of ^{18}F . In this work, we report on the development of ^{19}F -FCP and its ^{18}F -FCP analogue.

MATERIALS AND METHODS

Materials

All reagents and solvents were purchased from Sigma-Aldrich and used without further purification. Nuclear Magnetic Resonance (NMR) spectra (^1H -NMR, ^{13}C -NMR, and ^{19}F -NMR, ^{195}Pt -NMR) were obtained using Varian Mercury 300 MHz and Varian Inova 400 MHz spectrometers. Tetramethylsilane was used as an internal standard. Radio High

Performance Liquid Chromatography (HPLC) analysis was carried using a HPLC pump (Waters, Model 1525) equipped with ultraviolet detector (Waters, Model 2489) and radiation detector (Bio-scan, Model B-FC-3300). Radioactivity was measured with a dose calibrator (Captintec CRC-15 PET) and gamma counting was done using LKB Wallac 1282 counter.

Reference Compound ^{19}F -FCP

Synthesis of intermediates and ^{19}F -FPMA was performed as published in our previous literature (18). Cisplatin (0.2mmol) and silver nitrate (0.3mmol) were dissolved in nanopure water (2.5 mL) and the mixture was stirred at room temperature overnight in dark. After filtration of the precipitated silver chloride, one equivalent (0.2mmol) ^{19}F -FPMA **4** was added, and the mixture was stirred at room temperature for 2 days. Product was purified by solid phase extraction using quaternary methyl ammonium cartridge using water as eluent and the fractions were lyophilized to give ^{19}F -FCP **5** in 90% yield. ^1H -NMR (300 MHz) (D_2O) δ 1.32-1.47 (m, 4H), 1.49 (s, 3H), 1.65-1.78 (m, 2H), 1.90-1.94 (m, 2H), 4.50 (t, $J = 6.05$ Hz, 1H), 4.66 (t, $J = 6.05$ Hz, 1H) ; ^{19}F -NMR (300 MHz) (D_2O) δ -218.88 (m); ^{195}Pt -NMR (300 MHz) (D_2O) δ -1596 (broad singlet). ESI-MS $[\text{M} + \text{Na}]^+$ m/z calcd for $\text{C}_9\text{H}_{19}\text{FN}_2\text{O}_4\text{Pt} + \text{Na}$ 456.33, found 456.33.

Radiosynthesis and Characterization of ^{18}F -FCP

Synthesis of ^{18}F -FPMA was performed according to our previously published methods (18). The final ^{18}F -FPMA (3.3×10^4 MBq) was re-dissolved in water (0.25 mL) and aqua platinum complex (0.5 mL) was added to the radioactivity and the vial was heated at 75°C for 30 min. In the reaction, about 50% of the unreacted starting compound, ^{18}F -FPMA was observed by HPLC analysis. Final ^{18}F -FCP was purified by solid phase extraction using quaternary methyl ammonium Sep-Pak ion-exchange cartridge. Purification was carried out using water as a mobile phase and elution in 0.25 mL fractions. A total of seven

fractions were collected, and ^{18}F -FCP was eluted in fractions 2-4, with majority of the ^{18}F -FCP radioactivity eluted in fractions 3 and 4. ^{18}F -FPMA was not detected in any of the water eluted fractions, by HPLC analysis. Remaining radioactivity detected in the cartridge, was eluted with 0.5 mL ethanol and HPLC analysis of this sample showed ^{18}F -FPMA peak.

The automated synthesis of ^{18}F -FCP was conducted using AllinOne module (Trasis, SA). The AllinOne synthesizer was driven by interactive software. Synthesis of ^{18}F -FCP was programmed using in-house reaction sequences that were derived from manual synthesis to automate the steps that can be viewed in real time. The automated experiments were conducted using a range of activities (1.9×10^4 - 2.8×10^4 MBq of ^{18}F). The ^{18}F -fluorination reaction was optimized using the same parameters used in manual synthesis. Final samples were collected and radiochemical purity was analyzed using radio-HPLC. For *in vivo* studies, the required amount of activity was brought up to 200 μL volume with phosphate buffered saline for intravenous injection.

Cell Lines and Culture Conditions

All cell lines were maintained in a humidified incubator at 37 °C and 5% CO_2 . Human cervical epidermoid carcinoma (KB 3-1) was a generous gift from Dr. Michael Gottesman (NCI, National Institutes of Health, Bethesda, MD). Human Lung Carcinoma (A549), Ovarian Carcinoma (SK-OV-3), Colon Adenoarcinoma (COLO-205), Renal Carcinoma (A498) and Prostate Carcinoma (LNCap) cell lines were purchased from ATCC. Head and Neck Carcinoma (FaDu) cell line was a gift from Dr. Andrei Pugachev at Massey Cancer Center, Virginia Commonwealth University. KB-3-1 cells were grown in DMEM/high glucose medium supplemented with 10% fetal bovine serum (FBS), 5 mM L-Glutamine, Penicillin (100 U/mL), Streptomycin (100 $\mu\text{g}/\text{mL}$) and Amphotericin B (0.25 $\mu\text{g}/\text{mL}$). SK-OV-3, COLO-205, FaDu, A549, A498, LNCap cells were cultured in RPMI-1640 medium

supplemented with 10% heat inactivated FBS Penicillin G (100 U/mL), Streptomycin (100µg/mL) and Amphotericin B (0.25 µg/mL). The cells were grown to 70-80% confluency.

***In vitro* Cytotoxicity of ¹⁹F FCP**

The cytotoxicity of ¹⁹F-FCP to various cell lines was compared with that of cisplatin and carboplatin. The viability of COLO-205, SK-OV-3, FaDu, A549, A498, LNCaP, RWPE-1, and KB-3-1 cells, treated with cisplatin, carboplatin, or ¹⁹F-FCP, was evaluated. Cells plated in triplicates and grown in well plates were treated with 25 µL drug at final concentrations of 0.001 (µM) to 100 (µM) for 72 hours and 96 hours. At the end of incubation period, the cell viability was assessed using CellTiter-Glo assay kit (Promega, USA) and a plate reader (Beckman Coulter). The luminescence detected in untreated cells was used as control (100% Viability) to calculate percent viability in treatment groups. The percent viability of each cell line was plotted and used to calculate the inhibitory concentration 50 for each drug. Statistical analysis was done using student's t-test and the p value calculated based on two-tailed test using microsoft excel software.

Animals

Four to six weeks old female nude mice, from Harlan Laboratory (Indianapolis, IN, USA), were used for experimentation. Animal experiments were approved and performed according to the policies and guidelines of the Institutional Animal Care and Use Committee, at Virginia Commonwealth University.

Animal Tumor Xenograft

Tumor cells 2.5×10⁶/100 µL (KB 3-1), 2.5×10⁶/100 µL (COLO-205) in media without serum were injected subcutaneously into the right flank (KB3-1) and left shoulder

(COLO-205) of athymic nude mice (4-6 weeks old, weight: 18-25 g). Following subcutaneous implantation, digital caliper measurements of tumor size was accessed when the tumor was palpable at the injection site (approximately 5 days). The tumor volume was calculated using the formula $L \times W^2/2$ and assessed twice a week.

Biodistribution and *in vivo* Stability Analysis

The biodistribution of ^{18}F -FCP was measured in adult female nude mice. Under 2% isoflurane, four groups of three mice, each received an intravenous injection (tail vein) of ^{18}F -FCP (2.6-5.2 MBq, in 200 μL phosphate buffered saline). Under anesthesia, mice were sacrificed at 5, 30, 60 and 90 min post injection. Whole blood was collected, other major organs were harvested and weighed, and the radioactivity in the tissues was counted in a gamma counter (LKB Wallac 1282). The blood activity was used to calculate the blood half-life. Decay-corrected radiotracer uptake in each tissue at various time points was then calculated as the percent injected dose per gram of tissue (%ID/g).

In vivo stability of ^{18}F -FCP in plasma and urine was determined following radiotracer administration (2.6-5.2 MBq, in 200 μL phosphate buffered saline) in female nude mice under 2% isoflurane anesthesia. Samples were collected at 5, 30, 60, and 90 min following intravenous injection of ^{18}F -FCP. The collected samples of plasma were centrifuged for 10 min at 10,000g. Supernatants from these samples were filtered through 0.2 μm filter and 200 μL of filtrate was injected into reversed-phase HPLC (column Waters Nova-Pak 4 μm C18 150 \times 3.9 mm, ACN:H₂O 25:75, containing 0.1% trifluoroacetic acid at flow rate 1mL/min). Urine samples were also filtered and analyzed in the same HPLC system.

PET Imaging

Small animal PET/CT imaging studies were performed using a multimodality preclinical system (Siemens Medical Solutions Inc., Knoxville, TN, USA). Ten min prior to imaging, the animals were anesthetized with 2% isoflurane in oxygen. After sedation, the animal was placed onto the imaging bed and anesthesia was maintained for the duration of the imaging. A 90-minute dynamic scan was initiated and ^{18}F -FCP (5.5-6 MBq, in 200 μL phosphate buffered saline) was injected via its tail vein. The micro CT imaging was acquired following the PET imaging at 80kV and 500 μA with a focal spot of 58 μm .

PET images were reconstructed using Fourier Re-binning and Ordered Subsets Expectation Maximization 3D algorithm with dynamic framing sequence. Reconstructed PET/CT images were fused and analyzed using Inveon® Research Workplace software (IAW 1.6). For quantitation, regions of interest were drawn around areas of high radiotracer activity in each organ. The resulting quantitative data were expressed as %ID/g.

RESULTS

Synthesis of Cold Reference Standard Compound (^{19}F -FCP)

Fig. 1 describes the synthesis of the tosylated precursor and reference standard compound ^{19}F -FCP **5**. Fluorination of compound **5** was confirmed by ^{19}F -NMR, which showed the expected multiplet pattern and had a chemical shift in the expected region (218.88 for terminal (CH_2F). Chemical purity of compound **5** was found to be greater than 98% as determined by analytical HPLC.

Cytotoxicity of ^{19}F -FCP

Based on the cell viability data (Table 1), the inhibitory concentration 50 values for the various platinum compounds showed that cisplatin reduced the cell viability to a greater extent than carboplatin and ^{19}F -FCP, which is consistent with the greater toxicity of cisplatin

over carboplatin ($p < 0.05$). The relative cytotoxicity was similar across cell lines, but ^{19}F -FCP was slightly more potent than carboplatin. At 72 hours, the difference was significant in A549, KB3-1 and RWPE-1 cell lines ($p < 0.005$); but less so at 96 hours for all cell lines ($p < 0.05$). Cytotoxic effect for all three compounds was time dependent. Increasing the incubation time from 72 hours to 96 hours reduced the inhibitory concentration 50 values for all three compounds indicating an increase in cytotoxicity with time.

Radiosynthesis of ^{18}F -FCP

Fig. 2 represents the radiosynthesis of ^{18}F -FCP **8** in three steps: i) Kryptofix-mediated direct nucleophilic fluorination ii) NaOH Base Hydrolysis and iii) Co-ordination with Platinum Aqua Complex. The decay corrected yield of final product, 180 min after the introduction of ^{18}F -fluoride activity (isolated RCY of ^{18}F -FCP) was $14.3 \pm 3.8\%$ ($n=3$), and the radiochemical purity was more than 98%. Automation reduced the synthesis time by only 30 min which is plausible since the reaction steps were replicated from the manual procedures. The decay corrected yield of final product, 150 min after the introduction of ^{18}F -fluoride (isolated RCY of ^{18}F -FCP) was 16.2 ± 0.95 ($n=4$) and the radiochemical purity was more than 98% as confirmed by radio-HPLC. Retention time of ^{18}F -FCP was 1.43 min (Fig. 3) which was distinguishable from the free fluoride (retention=0.7-0.8 min) under these conditions. It has been previously reported (21) that retention of free fluoride is variable depending on column characteristics and mobile phase constituents.

Biodistribution and *in vivo* Stability Analysis

Fig. 4 shows the biodistribution of ^{18}F -FCP in female nude mice. The radiotracer demonstrated rapid blood clearance with less than 2% of radioactivity remaining in the

circulation after 1 h. The blood half-life was calculated to be 16 min. Most organs showed low accumulation of the radiotracer and radioactivity was predominantly cleared through the kidneys with greater than 95% cleared 1 hour after injection.

The *in vivo* stability of ^{18}F -FCP in plasma and urine was assessed during the first 60 min after intravenous administration in normal nude mice. The stability of ^{18}F -FCP was determined by radio-HPLC at 5, 30, 60, and 90 min post administration. The radio-HPLC peak of the plasma samples injected appeared at the same retention time as the initial injected radiotracer (Fig. 5), demonstrating an intact ^{18}F -FCP 60 min-post injection. No radioactivity was detected in 90 minute samples, which could be attributed to the fast-physiological clearance of the radiotracer from the blood. The radio HPLC peak of the urine samples injected also appeared at the same retention time as the initial injected radiotracer demonstrating the intact ^{18}F -FCP (Supplemental Fig. 1).

PET Imaging

Dynamic images acquired for 90 min illustrate the full body distribution of ^{18}F -FCP (Fig. 6). ^{18}F -FCP had the highest uptake in kidneys. Accumulation of radiotracer was also seen in lungs and liver in early time points. High uptake in the kidneys seems to reflect urinary excretion of the tracer, which can be attributed to the radioactivity present in the urine during the scan. Images showed the subsequent clearance of radiotracer with time. Static images acquired 90 min post radiotracer administration illustrate the full body distribution of ^{18}F -FCP in tumor bearing mice (Fig. 7). Major uptake was observed in liver and abdominal region. Region of interest analysis showed that KB 3-1 tumor has higher uptake (2.6 %ID/g) than COLO-205 (0.8 %ID/g). The inset image of Fig. 7 also showed clear heterogeneous uptake in the KB 3-1 tumor.

DISCUSSION

Reduced intracellular drug accumulation has been identified as a major factor associated with drug resistance (10). A direct *in vivo* measure of drug in tumors is therefore an important means to address this issue. PET imaging with radiolabeled drug provides a non-invasive direct measure of intra-tumor drug distribution. This can then be related to the detection of any proteome alterations that may have contributed to the degree of regional drug uptake, retention, or efflux, culminating in drug resistance. Radiolabeled platinum drugs have been synthesized with platinum radioisotopes as radioactive drugs for imaging and therapy studies. Areberg et al (11) studied the antitumor effect of radioactive cisplatin (^{191}Pt) in tumor bearing nude mice and demonstrated that [^{191}Pt]-cisplatin is more effective than unlabeled cisplatin in retarding tumor growth. Patient studies by Areberg et al (22,23) demonstrated the use of cisplatin radiolabeled with ^{191}Pt , $^{193\text{m}}\text{Pt}$, or $^{195\text{m}}\text{Pt}$ to visualize the uptake of platinum in tumor and tissues non-invasively after cisplatin treatment. Dowell et al (13) used $^{195\text{m}}\text{Pt}$ labeled cisplatin and carboplatin to estimate, through imaging, the amount of drug at the tumor site and at selected organs. However, the production and supply of platinum radionuclides is limited, and costly because of the need to use enriched platinum isotopes as target material, and the logistics of radiosynthesis (13). These factors did not facilitate wide applications of radio-platinum-labeled drugs. Positron-emitting radionuclide labeled drugs, and specifically ^{18}F -labeled drugs, represent a feasible strategy to develop PET imaging that can be clinically applied to evaluate biodistribution of drugs.

In this work, we developed FCP as a drug analogue to carboplatin and ^{18}F -FCP as a companion imaging diagnostic agent. Such development represents an advance over previous work using platinum or nitrogen radionuclides for labeling and imaging. We have demonstrated that the non-radioactive FCP analogue is at least as potent as the parent drug in various cancer cell lines *in vitro*. It remains to be seen whether the *in vivo* anti-

tumor effects of the analogue is as good as or better than that of carboplatin. Therapeutic studies to address this are underway and the findings will be reported in a separate manuscript. We show that ^{18}F -FCP biodistribution profile, by PET imaging, is like the previously reported overall pharmacokinetic data for carboplatin (24-26). The radiotracer is stable in plasma and urine at 60 min after administration (Fig. 5). There appears to be a small peak at about 5.3 minutes in the plasma HPLC chromatogram, which could be attributed to a metabolite, but the presence or lack thereof of this needs to be confirmed in future studies. ^{18}F -FCP exhibited distribution throughout the body and the blood clearance pattern followed mono-exponential blood kinetics. The blood half-life of ^{18}F -FCP was calculated to be 16 min which is similar to reported value for carboplatin (26). Following intravenous injection of ^{18}F -FCP in normal nude mice, quantification of the dynamic images up to 90 min post injection, showed highest activity in kidneys, bladder and urine. Accumulation of ^{18}F -FCP was also recorded in liver and lungs in early time points with subsequent clearance with time which is consistent with the findings by Ginos et al (15) for ^{13}N -labeled cisplatin. Ex-vivo biodistribution data corresponded to the imaging results with major accumulation of radiotracer in kidneys and liver (Fig. 4).

The data generated herein showed that ^{18}F -FCP PET/CT can be used to non-invasively assess drug distribution profile in different tumor types. ^{18}F -FCP uptake in KB-3-1 tumor was much higher than that in COLO-205 tumor. Furthermore, PET imaging revealed that the uptake in the KB-3-1 tumor is heterogeneous with significant differences in uptake in different tumor regions. In this work, we demonstrate that ^{18}F -FCP PET/CT is a unique tool that can measure intra-tumor heterogeneous drug distribution. This information can be useful, when combined with proteomic analysis to better understand the relationship between intra-tumor drug distributions, proteome alterations in distinct tumor regions, drug-tumor interaction, mechanisms of resistance and tumor recurrence.

^{18}F -FCP could also depict kinetics of drug efflux which is related to drug resistance. Although many anti-cancer drugs are widely used in the clinic, many questions remain unanswered about how individual patient tumors interact with drugs and how much actual drug is being retained in different tumors, both leading to the question why patients with the same type of tumor respond differently to the same drug treatment. PET using radiolabeled drugs is the only imaging method that could further our understanding of the clinical behavior of drug therapy, and may contribute to better guided treatment planning in individual patients.

CONCLUSION

The synthesis of a fluorinated analogue of carboplatin was developed. The compound retains anti-tumor activity of parent drug. The feasibility to produce ^{18}F -FCP, for PET imaging, was demonstrated. The pharmacokinetics of ^{18}F -FCP mirrors that of carboplatin and the profile shows major accumulation in kidneys and liver. This PET tool enabled imaging of intra-tumor drug distribution and enabled the detection of heterogeneous retention within the tumor. The development of ^{18}F -FCP PET represents a novel tool which can be used to image-guide platinum therapy with the aim of enhancing overall efficacy of platinum-based chemotherapy on individualized patient basis.

DISCLOSURE

The authors declare no conflicts of interest.

ACKNOWLEDGEMENTS

This work was supported by Virginia Commonwealth University School of Medicine. The authors would like to thank Bob Ylimaki, IBA Molecular for ^{18}F -fluoride production and Michael D'Cona for technical assistance.

REFERENCES

1. Rosenberg B, VanCamp L, Trosko JE, Mansour VH. Platinum compounds: a new class of potent antitumour agents. *Nature*. 1969;222:385-386.
2. Howell SB, Safaei R, Larson CA, Sailor MJ. Copper transporters and the cellular pharmacology of the platinum-containing cancer drugs. *Mol Pharmacol*. 2010;77:887-894.
3. Rabik CA, Maryon EB, Kasza K, Shafer JT, Bartnik CM, Dolan ME. Role of copper transporters in resistance to platinating agents. *Cancer Chemother Pharmacol*. 2009;64:133-142.
4. Gately DP, Howell SB. Cellular accumulation of the anticancer agent cisplatin: a review. *Br J Cancer*. 1993;67:1171-1176.
5. Stewart DJ. Mechanisms of resistance to cisplatin and carboplatin. *Crit Rev Oncol Hematol*. 2007;63:12-31.
6. Johnstone TC, Park GY, Lippard SJ. Understanding and improving platinum anticancer drugs--phenanthriplatin. *Anticancer Res*. 2014;34:471-476.
7. Wang AZ, Langer R, Farokhzad OC. Nanoparticle delivery of cancer drugs. *Annu Rev Med*. 2012;63:185-198.
8. Holohan C, Van Schaeybroeck S, Longley DB, Johnston PG. Cancer drug resistance: an evolving paradigm. *Nat Rev Cancer*. 2013;13:714-726.
9. Moreno-Smith M, Halder JB, Meltzer PS, et al. ATP11B mediates platinum resistance in ovarian cancer. *J Clin Invest*. 2013;123:2119-2130.

10. Shen DW, Pouliot LM, Hall MD, Gottesman MM. Cisplatin resistance: a cellular self-defense mechanism resulting from multiple epigenetic and genetic changes. *Pharmacol Rev.* 2012;64:706-721.
11. Areberg J, Wennerberg J, Johnsson A, Norrgren K, Mattsson S. Antitumor effect of radioactive cisplatin (¹⁹¹Pt) on nude mice. *Int J Radiat Oncol Biol Phys.* 2001;49:827-832.
12. Baer J, Harrison R, McAuliffe CA, Zaki A, Sharma HL, Smith AG. Microscale syntheses of anti-tumour platinum compounds labelled with ¹⁹¹Pt. *Int J Appl Radiat Isot.* 1985;36:181-184.
13. Dowell JA, Sancho AR, Anand D, Wolf W. Noninvasive measurements for studying the tumoral pharmacokinetics of platinum anticancer drugs in solid tumors. *Adv Drug Deliv Rev.* 2000;41:111-126.
14. Lind MJ, Murphy DJ, Sharma H, et al. Comparative intraperitoneal pharmacokinetics of three platinum analogues. *Cancer Chemother Pharmacol.* 1991;28:315-317.
15. Ginos JZ, Cooper AJ, Dhawan V, et al. [¹³N]cisplatin PET to assess pharmacokinetics of intra-arterial versus intravenous chemotherapy for malignant brain tumors. *J Nucl Med.* 1987;28:1844-1852.
16. De Spiegeleer B, Slegers G, Vandecasteele C, et al. Microscale synthesis of nitrogen-13-labeled cisplatin. *J Nucl Med.* 1986;27:399-403.
17. Moker J, Thiem J. Synthesis and hydrolysis studies of novel glyco-functionalized platinum complexes. *Carbohydr Res.* 2012;348:14-26.
18. Dewkar GK, Sundaresan G, Lamichhane N, et al. Microfluidic radiosynthesis and biodistribution of [¹⁸F] 2-(5-fluoro-pentyl)-2-methyl malonic acid. *J Labelled Comp Radiopharm.* 2013;56:289-294.
19. Ogawa K, Aoki M. Radiolabeled apoptosis imaging agents for early detection of response to therapy. *ScientificWorldJournal.* 2014;2014:732603.

- 20.** Knox RJ, Friedlos F, Lydall DA, Roberts JJ. Mechanism of cytotoxicity of anticancer platinum drugs: evidence that cis-diamminedichloroplatinum(II) and cis-diammine-(1,1-cyclobutanedicarboxylato)platinum(II) differ only in the kinetics of their interaction with DNA. *Cancer Res.* 1986;46:1972-1979.
- 21.** Ory D, Van den Brande J, de Groot T, et al. Retention of [(18)F]fluoride on reversed phase HPLC columns. *J Pharm Biomed Anal.* 2015;111:209-214.
- 22.** Areberg J, Bjorkman S, Einarsson L, et al. Gamma camera imaging of platinum in tumours and tissues of patients after administration of 191Pt-cisplatin. *Acta Oncol.* 1999;38:221-228.
- 23.** Areberg J, Norrgren K, Mattsson S. Absorbed doses to patients from 191Pt-, 193mPt- and 195mPt-cisplatin. *Appl Radiat Isot.* 1999;51:581-586.
- 24.** Siddik ZH, Newell DR, Boxall FE, Harrap KR. The comparative pharmacokinetics of carboplatin and cisplatin in mice and rats. *Biochem Pharmacol.* 1987;36:1925-1932.
- 25.** Ueda T, Yasumasu T, Uozumi J. Experimental studies on the pharmacokinetics and nephrotoxicity of carboplatin (cis-diammine-1, 1-cyclobutane dicarboxylate platinum II) in rats. *J Toxicol Sci.* 1991;16:101-109.
- 26.** van Hennik MB, van der Vijgh WJ, Klein I, et al. Comparative pharmacokinetics of cisplatin and three analogues in mice and humans. *Cancer Res.* 1987;47:6297-6301.

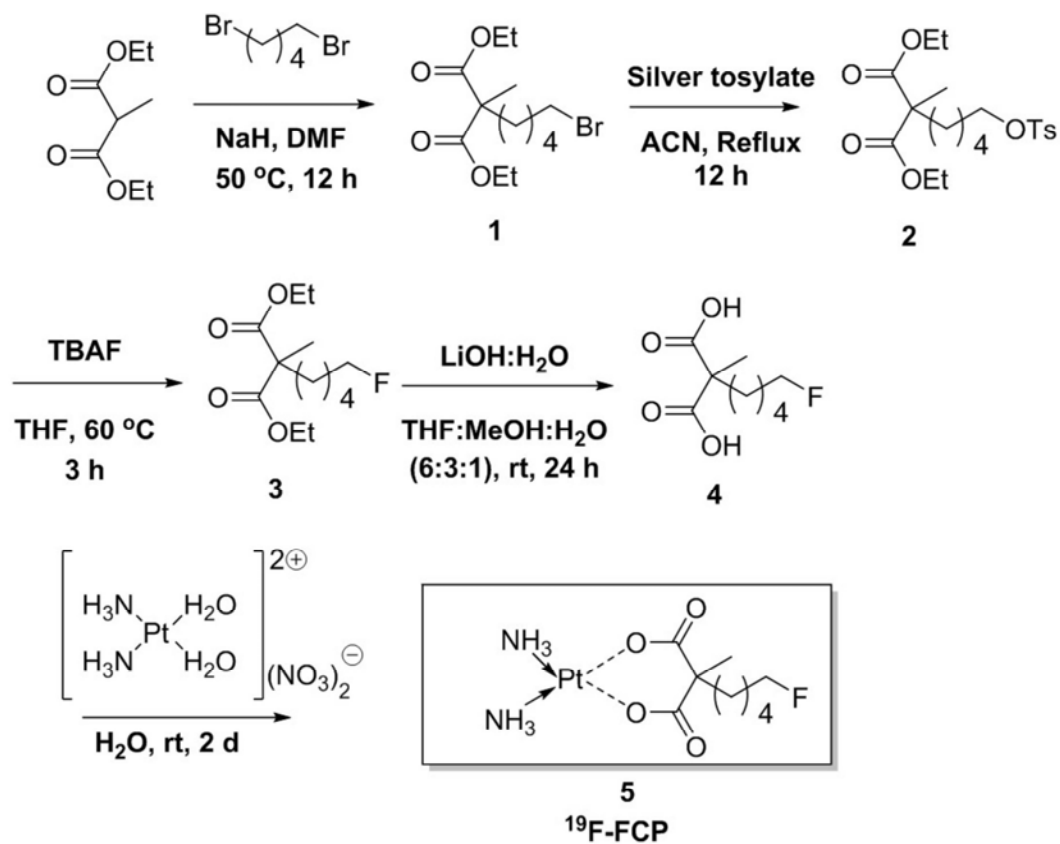


FIGURE 1: Reagents and conditions: (a) 1,5-dibromopentane, NaH, DMF, 50 °C, 12 h, 72%; (b) silver tosylate, ACN, reflux, 12 h, 96%; (c) TBAF, THF, 60 °C, 3 h, 84%; (d) LiOH/H₂O THF/MeOH/H₂O (6:3:1), rt, 24 h, 86% (e) platinum aqua complex, rt, 2 days.

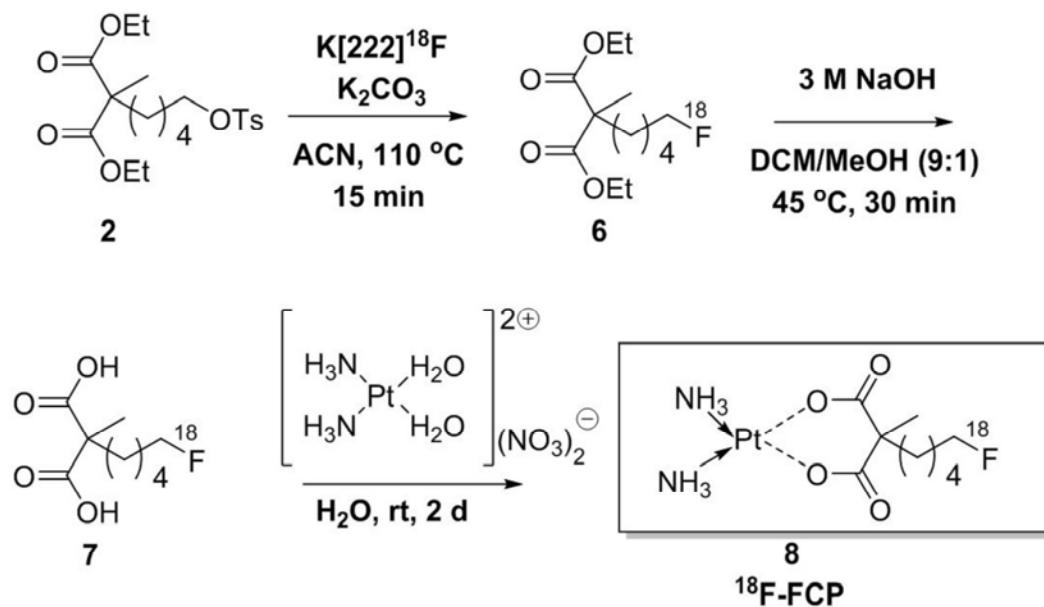


FIGURE 2: Reagents and conditions: (a) $\text{K}^{18}\text{F}/\text{K}_{222}$, K_2CO_3 , ACN, $110\text{ }^\circ\text{C}$, 10 min condition used for manual synthesis; (b) glass microfluidic device, $\text{K}^{18}\text{F}/\text{K}_{222}$, K_2CO_3 , ACN, $190\text{ }^\circ\text{C}$, condition used in automated microfluidic synthesis; (c) 3 mol NaOH, DCM/MeOH (9:1), $45\text{ }^\circ\text{C}$, 20 min; (d) 3 M HCl, in manual and sodium citrate buffer (pH 2.79) in microfluidic synthesis, was used for pH adjustment (pH 2–3), (e) platinum aqua complex, $82\text{ }^\circ\text{C}$, 30 min.

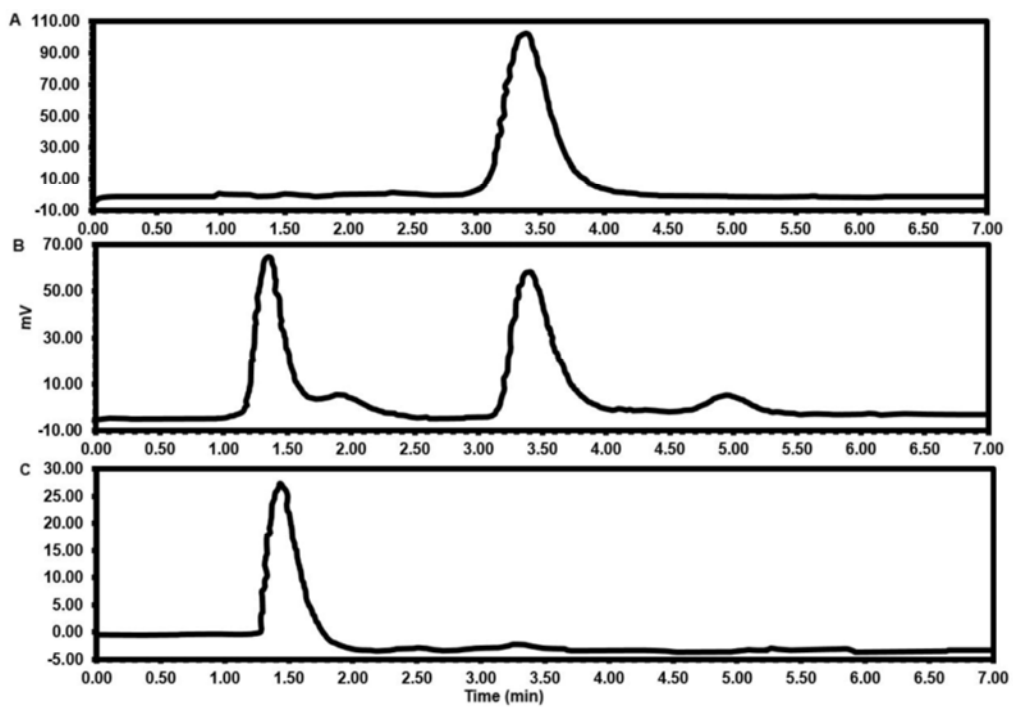


FIGURE 3: Radio-HPLC analysis of radiosynthesis steps and the purified final product. Sample was run on Waters® 4 μ C18 150 x 3.9 mm column; ACN/Water (0.1% trifluoroacetic acid) 25/75 with flow rate of 1mL/min. **A:** ^{18}F -FPMA (RT = 3.38 min); **B:** Sample taken from platinum coordination reaction before purification; **C:** Sample taken from ^{18}F -FCP product (RT=1.43 min).

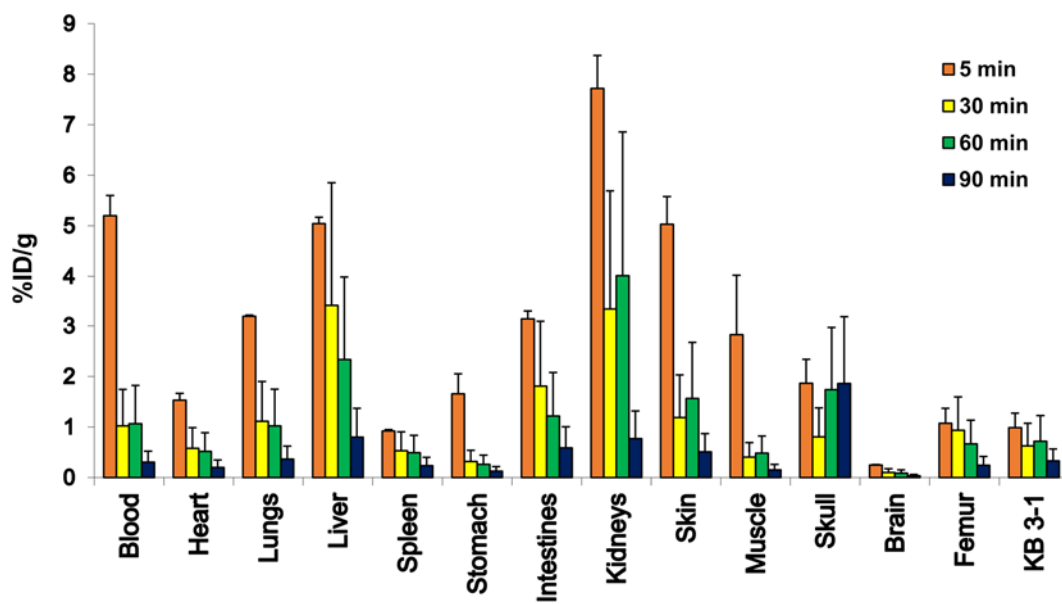


FIGURE 4: Biodistribution of ^{18}F -FCP in KB 3-1 tumor bearing adult female nude mice ($n=3/\text{time point}$) at 5, 30, 60, 90 min after intravenous injection. Radio tracer uptake in % ID/g was determined by gamma counting. KB-3-1 = Cervical Tumor Xenograft.

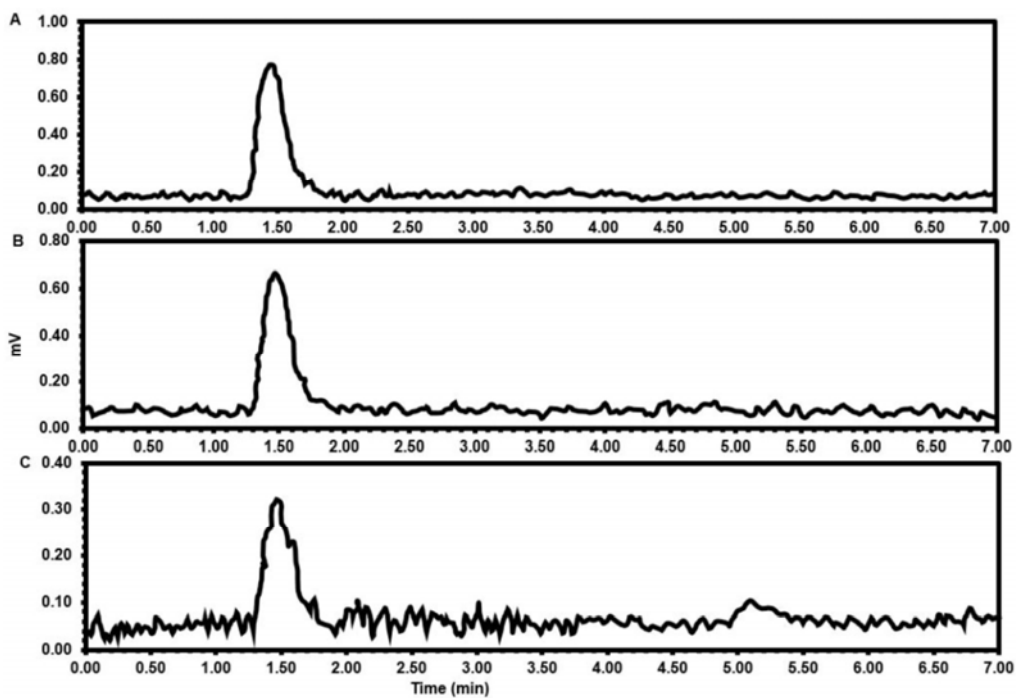


FIGURE 5: Radio-HPLC analysis of plasma samples run on Waters® 4 μ C18 150 x 3.9 mm column; ACN/Water (0.1% trifluoroacetic acid) 25/75 with flow rate of 1mL/min at different time points after i.v. injection; **A:** 5 min; **B:** 30 min; **C:** 60 min.

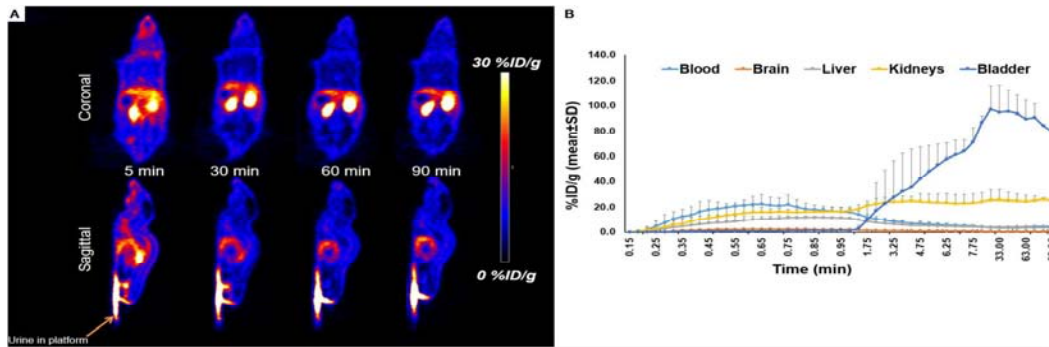


FIGURE 6: A female nude mouse was injected (i.v) with 5.5-6 MBq of ^{18}F -FCP and imaged using Inveon PET/CT scanner. (A) Selected slices of dynamic image data that was acquired for up to 90 min.(B) Time-activity curve data generated from the dynamic image dataset that shows the time dependent kinetics and tissue clearance.

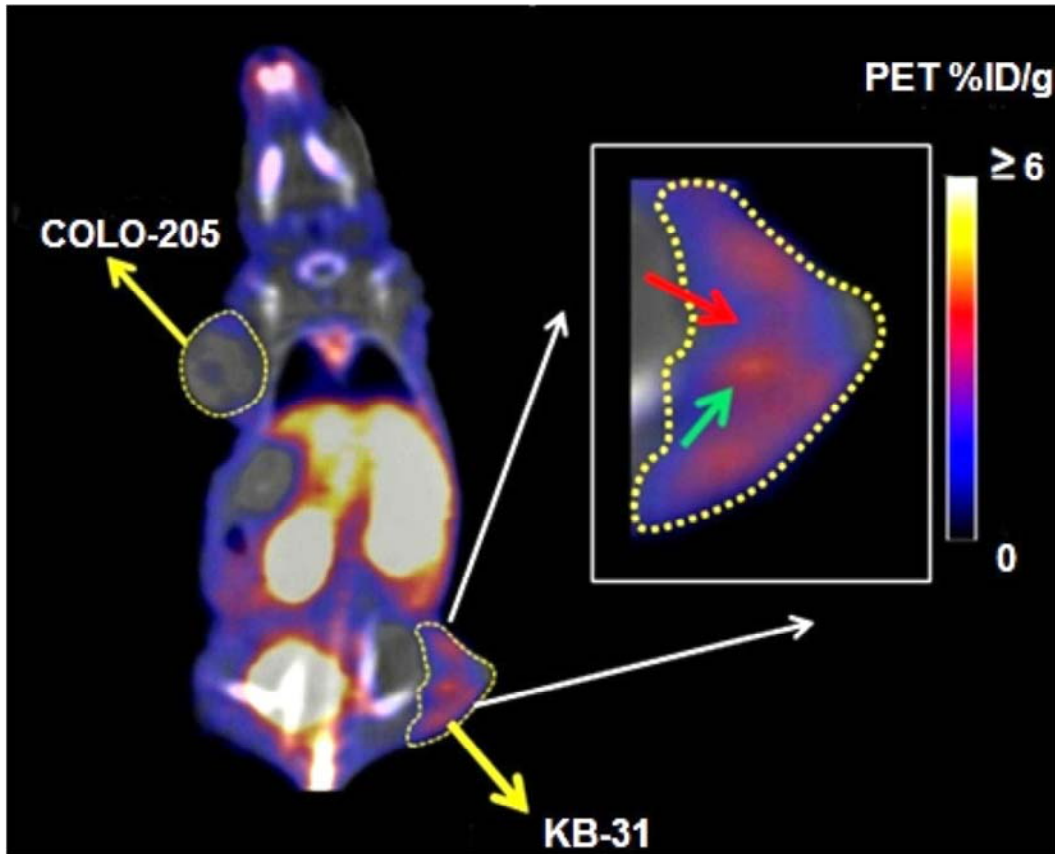
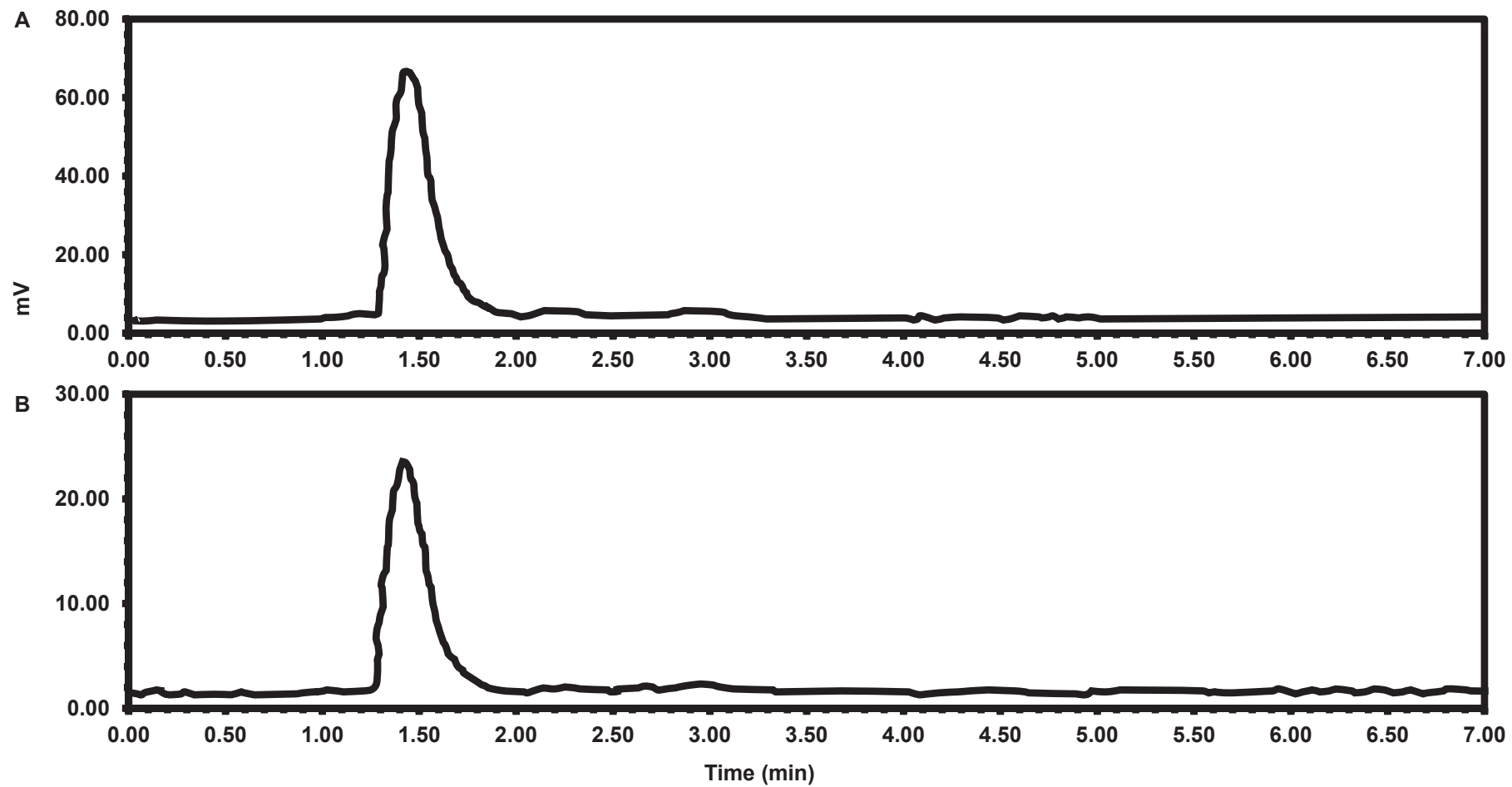


FIGURE 7: ^{18}F -FCP (5.5-6 MBq) was injected intravenously via tail vein in a nude mouse bearing a KB 3-1 and a COLO-205 xenografts. Imaging was carried out 90 min post injection using Inveon PET/CT and the static image was reconstructed and analyzed. Images showed obvious difference in uptake of ^{18}F -FCP between KB 3-1 (2.6% ID/g) and COLO-205 tumors (0.8 %ID/g). Furthermore, the heterogeneity of the uptake was evident in the KB-3-1 tumor (inset), showing regions of high (cyan arrow) and low (red arrow) ^{18}F -FCP uptake. This observation is now being further investigated in our laboratory using carboplatin sensitive (A2780) and resistant (A2780-CP20) tumor models.

TABLE 1: IC₅₀ values of Cisplatin, Carboplatin and ¹⁹F-FCP in various cancer cell lines.

Cell line	Cisplatin (μ M)		Carboplatin (μ M)		¹⁹ F-FCP (μ M)	
	72 hours	96 hours	72 hours	96 hours	72 hours	96 hours
COLO-205	25.72 \pm 4.32	6.68 \pm 7.54	>100	49.37 \pm 0.56	69.66 \pm 32.33	27.38 \pm 5.91
SK-OV-3	12.71 \pm 11.84	1.76 \pm 0.69	63.92 \pm 42.74	17.48 \pm 2.06	27.34 \pm 9.96	13.21 \pm 0.93
FaDu	4.38 \pm 2.28	1.22 \pm 0.59	45.78 \pm 15.65	12.38 \pm 1.59	27.53 \pm 8.47	8.1 \pm 0.64
A549	11.24 \pm 0.33	4.95 \pm 2.67	59.76 \pm 4.53	36.25 \pm 6.33	37.74 \pm 4.86	26.57 \pm 2.51
A498	13.35	5.47 \pm 2.90	>100	40.62 \pm 1.82	45.73 \pm 16.29	21.77 \pm 4.62
LNCaP	15.87 \pm 4.7	11.34 \pm 5.88	>100	74.41 \pm 15.57	64.72 \pm 21.73	73.83 \pm 39.27
KB 3-1	2.98 \pm 1.67	3.08 \pm 1.48	56.16 \pm 5.18	27.28 \pm 1.70	19.3 \pm 4.89	12.88 \pm 0.82
RWPE-1	9.11 \pm 4.02	12.83 \pm 0.10	88.94 \pm 33.59	59.96 \pm 1.06	36.23 \pm 2.18	39.76 \pm 0.40

IC₅₀ = Inhibitory Concentration 50.



Supplemental Figure 1: Radio-HPLC of urine samples run on Waters® 4 μ C18 150 x 3.9 mm column; ACN/Water (0.1% trifluoroacetic acid) 25/75 with flow rate of 1mL/min at different time points after i.v. injection; **A:** 5 min; **B:** 30 min.